EXPERIMENTAL AND COMPUTATIONAL INVESTIGATION OF SHOCK WAVE-TO-BUBBLY WATER MOMENTUM TRANSFER

K. A. Avdeev[1,2], V. S. Aksenov[1,2,3], A. A. Borisov[1,2,3], F. S. Frolov[1,2], S. M. Frolov[1,2,3], I. O. Shamshin[1,2,3], R. R. Tukhvatullina[2], B. Basara[4], W. Edelbauer[4], and K. Pachler[4]

[1]N. N. Semenov Institute of Chemical Physics
Russian Academy of Sciences
4 Kosygin Str., Moscow 119991, Russia
e-mail: smfrol@chph.ras.ru

[2]Center of Pulse Detonation Combustion
4 Kosygin Str., Moscow, Russia

[3]National Research Nuclear University "MEPhI"
(Moscow Engineering Physics Institute)
31 Kashirskoe Sh., Moscow 115409, Russia

[4]AVL LIST GmbH
1 Hans-List-Platz, Graz A-8020, Austria

Momentum transfer from shock waves (SWs) of various intensity (from 0.05 to 0.5 MPa in amplitude) to water containing air bubbles 2.5 mm of mean diameter is studied both experimentally and by means of numerical simulation. The experiments are performed in a vertical shock tube of a 50×100 mm rectangular cross section consisting of a 495-millimeter long high-pressure section (HPS), 495-millimeter long low-pressure section (LPS), and 990-millimeter long test section (TS) equipped with an air bubbler and filled with water. The experiments have shown that as the gas volume fraction in water increases from 0 to 0.3, the momentum imparted in bubbly water by shock waves increases monotonically, gradually leveling off at an air volume fraction of about 0.20–0.25. The experimental data are confirmed by two-dimensional (2D) simulation of SW propagation in bubbly water both

in terms of the SW velocity vs. the air content and the particle velocity behind the shock front.

Introduction

The thermodynamic cycle with burning in controlled detonation regime (Zel'dovich cycle) is known to provide a higher thermodynamic efficiency (performance) of fuel chemical energy transformation into the expansion work as compared to deflagration burning at constant volume [1, 2]. Although the use of the Zel'dovich cycle in liquid rocket engines and air-breathing jet engines was considered in numerous publications (see, for example, review [3] and references therein), the feasibility of utilization of this cycle in hydrojet engines was previously discussed solely in [4–7] to the best of our knowledge. According to [4–7], pulsed detonation hydrojet engine consists of a water passage and a generator of detonation waves fed with any suitable fuel mixture. The efficient momentum transfer to the fluid from a shock (or detonation) wave entering the water passage from the generator is the most important problem to be solved when realizing the Zel'dovich cycle in hydrojet engines.

The parameters of shock waves transmitted from a gas to bubbly water were studied usually in vertical shock tubes comprising HPS and LPS separated with a diaphragm and a TS with water containing air bubbles [8–12]. After the diaphragm at the top of LPS filled, as a rule, with air at atmospheric pressure and room temperature bursts, an SW with known parameters is formed which spreads through LPS and then enters the bubbly water. The velocity and other characteristics of the SW in bubbly liquid were monitored with pressure gauges mounted in the TS and with high-speed videocamera through the transparent windows in TS.

In the literature, one can find some other experimental data on SW propagation in bubbly liquids (see, e. g., [13, 14]); however, their quantitative analysis presents difficulties because some important parameters of experiments are missing in them. In addition, in many works, the experiments were performed with gases other than air (such as argon, helium, CO_2, etc.) in bubbles and liquids other than water (such as vacuum oil, water–glycerol mixture, boiling water or other) rather than water under normal conditions were used as a carrier medium. In

some works (see, e. g., [15]), SW was initiated by applying high-voltage (about 4–8 kV) to a thin wire submerged in bubbly liquid. Such works are not mentioned here because they have no relevance to the main objective of the present paper.

It should be noted that depending on governing parameters of the medium (viscosity and other), SW in bubbly water can have various pressure profiles [11, 16, 17], namely, with a smooth pressure time history or oscillatory. Experimental pressure traces recorded in [11] in SW spreading in water containing air bubbles of various size: 0.48, 0.69, or 0.1 mm at a similar gas volume fraction ~ 0.08 show that pressure behind the SW front in water with large bubbles oscillates intensely, whereas in water with small bubbles, the pressure profile is smooth [16, 17].

In [18–21], the interaction of bubbles with SW in bubbly liquids was studied experimentally and computationally. It has been found that bubbles are deformed and fragmented behind propagating SW due to instability of the gas–liquid interface.

The theoretical and computational studies of shock and detonation waves in bubbly liquids are usually based on one-dimensional partial differential equations of mass, momentum, and energy conservation for two mutually penetrating continua — liquid and gas [11, 22]. These equations are supplemented with semiempirical relationships for interphase dynamic and thermal interactions due to interphase velocity slip and temperature differences induced by the propagating SW such as: bubble deformation, fragmentation and coalescence, liquid evaporation, vapor condensation, interphase heat transfer, etc. The existing theoretical models of two-phase flows describe on the whole satisfactorily pressure wave propagation in bubbly liquids. As far as experimental and computational studies of SW – bubbly liquid interaction are concerned, the problem that has escaped attention of researches and calls for more detailed investigations because of its tentative practical importance is the efficiency of momentum transfer from an SW incident on a surface of a bubbly liquid to its bulk.

The objective of the present work is to study, both experimentally and by calculations, the impact of SW spreading in a gas onto a compressible bubbly water and to ascertain such an air content in water at which the momentum transfer from SW to bubbly water is the most efficient.

Experimental Setup and Methodology

The experiments were performed in laboratory setup called "Hydroshock tube" (HST) of a constant 50 × 100 mm rectangular cross section 1980 mm in total length (Fig. 1). The tube consists of a 495-

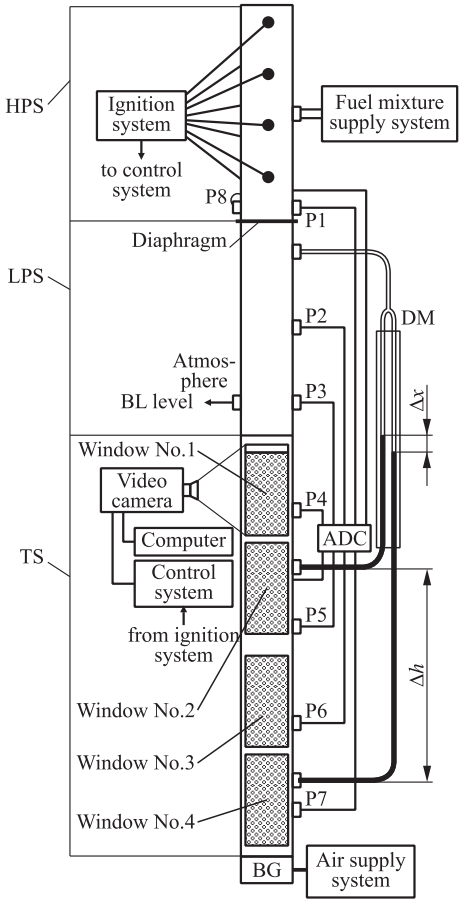

Figure 1 Schematic of the HST: BG — bubble generator; DM — differential manometer; BL — bubbly liquid; P1–P7 — piezoceramic gauges of overpressure, and P8 — absolute pressure transducer

millimeter long HPS, 495-millimeter long LPS, and 990-millimeter long TS filled with water. The experimental rig included a system that provides mixing of combustible gases, their supply to HPS and ignition, generator of bubbles mounted at the TS bottom end and manufactured in the form of a plate with 171 capillaries organized in equally spaced grid of 9 by 19 needles 0.16 mm in internal diameter, and data acquisition and control system. Air injected in water through the capillaries produced an array of bubbles. Pressure at the gas – bubbly liquid interface is atmospheric because LPS is connected to the ambient atmosphere through an orifice in the side wall 3 mm in diameter.

The overpressure in an SW was measured with a high-frequency piezoceramic pressure transducers PCB 113B24 — gauges P1 to P7 in Fig. 1. Absolute pressure in HPS was measured with a low-frequency KURANT-DA pressure transducer — gauge P8 in Fig. 1. The basic parameters of SW in air in LPS (its amplitude, duration, and propagation velocity) formed after the diaphragm was ruptured were derived from pressure traces recorded by pressure gauges P2 and P3. To visually monitor SW impact on a bubbly liquid, four optical windows were mounted in TS; in addition, visual observations were supplemented by pressure signals recorded with four pressure gauges P4 to P7. The signals from all pressure gauges P1–P8 were recorded via an R-Technology QMbox QMS20 analog-to-digital converter with the aid of the Power Graph 3.3 Professional program incorporated in a personal computer.

The positions of pressure gauges P1–P8 with respect to the diaphragm (see Fig. 1) and the depths with respect to the gas – bubbly liquid interface (its position was maintained at the same level in all tests) at which the gauges are located are indicated in the table.

Positions of pressure gauges P1–P8 with respect to the diaphragm and depths at which pressure gauges P4–P7 are located (from the liquid interface to the axial gauge line)

Gauge	Coordinate, mm	Depth, mm
P1, P8	−32	—
P2	247	—
P3	422	—
P4	673	135
P5	943	405
P6	1168	630
P7	1371	833

Volumetric air fraction in the water column was assessed by a change in the bubbly–liquid interface level (optical window No. 1 in

Fig. 1 had special marks for that purpose) or by a difference of liquid levels in a differential liquid manometer (see Fig. 1).

In the present work, interaction of SW with gas-containing liquid was studied at two different SW intensities: "weak" waves were about 0.05 MPa in amplitude and "strong" waves were about an order of magnitude more intense.

In tests with "weak" SW, a 25-micron thick diaphragm from polyethylene terephthalate (PET) was used. The air pressure in HPS at the diaphragm rupture instant was ~ 0.3 MPa.

"Strong" SWs were produced using 150-micron thick diaphragms which were stuck from three sheets of a 50-micron PET film, the HPS gas pressure at the diaphragm burst instant in these experiments at a level of ~ 1.5 MPa was attained by burning a propane–air mixture enriched with oxygen (up to 30 %(vol.)). Low-pressure section was filled with air at atmospheric pressure in all tests. Test section contained a (940 ± 15)-millimeter high water column with air bubbles of mean diameter $d_{10} = 1.5$–3.5-millimeter varied with the volumetric gas content from 0.005 to 0.3. In all tests, air and water were at room temperature.

To achieve a good spatial resolution, bubbly liquid was photographed just before each experiment by a Canon EOS 700D photocamera. Figure 2 shows a representative photo used to ascertain the size distribution of bubbles in one of the tests with a polyethylene thread. In this particular test, the mean bubble diameter was 2.5 mm and the diameters of fine and coarse fractions were 1.6 and 4 mm, respectively. It is noteworthy that as the volumetric gas content increases, so does the mean diameter of bubbles and the bubble shape becomes more irregular. Besides air bubbles, one can see in Fig. 2 scale marks (*1*) used to measure the height along TS (the distance between the horizontal scale bars is 20 mm), a twisted twin polyethylene thread of 1 mm in diameter (*2*) fixed at copper holders (*4* and *5*) with the aid of a fluorocarbon fishing line of 0.11 mm in diameter (*6*), and a thick horizontal (*3*) line indicating the initial thread position. The polyethylene thread was used due the proximity of its density to water density. Thread motion was monitored to assess the bubbly liquid velocity.

The velocities of the gas–liquid interface (contact surface) and air bubbles were obtained using Phantom Camera Control software during postprocessing of videoframes taken with a high-speed Phantom Miro

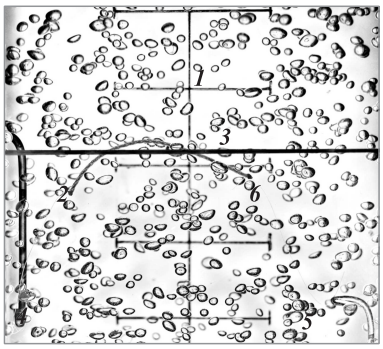

Figure 2 An example of photograph of window No. 2 with a polyethylene thread used to measure the liquid flow velocity ($\alpha_{10} \approx 0.01$): *1* — horizontal background scale marks following with 20-millimeter step; *2* — polyethylene thread; *3* — reference line equidistant from gauges P4 and P5 at 135 mm; *4* and *5* — the holders of the thread; and *6* — a fluorocarbon fishing line

LC310 camera. The positions and velocities of several selected points in videoframes were measured after preliminary calibration, which ascertains the scale relation between a real physical object (e. g., dimension mesh drawn on the TS window, see Fig. 2) and its image. Air bubbles are involved in motion behind an SW and can be disintegrated. To take into account this phenomenon, one has to manually "teach" the trace algorithm. As a result, the algorithm can trace the position of a cluster of smaller bubbles formed from the parent bubble as a result of its breakup.

Figures 3 and 4 demonstrate representative oscilloscopic traces of signals from gauges P2–P7 used to measure the average SW velocity (D) at measuring segments P2–P3, P3–P4, P4–P5, P5–P6, and P6–P7:

$$D_{ij} = \frac{X_j - X_i}{\tau_j - \tau_i}$$

where ij is the pressure gauge number (see Fig. 1), X_j and X_i are the coordinates of gauges i and j (see the table); and $(\tau_j - \tau_i)$ is the time interval during which the SW front travels between gauges i and j. The instant SW arrived at one or another pressure gauge was determined as

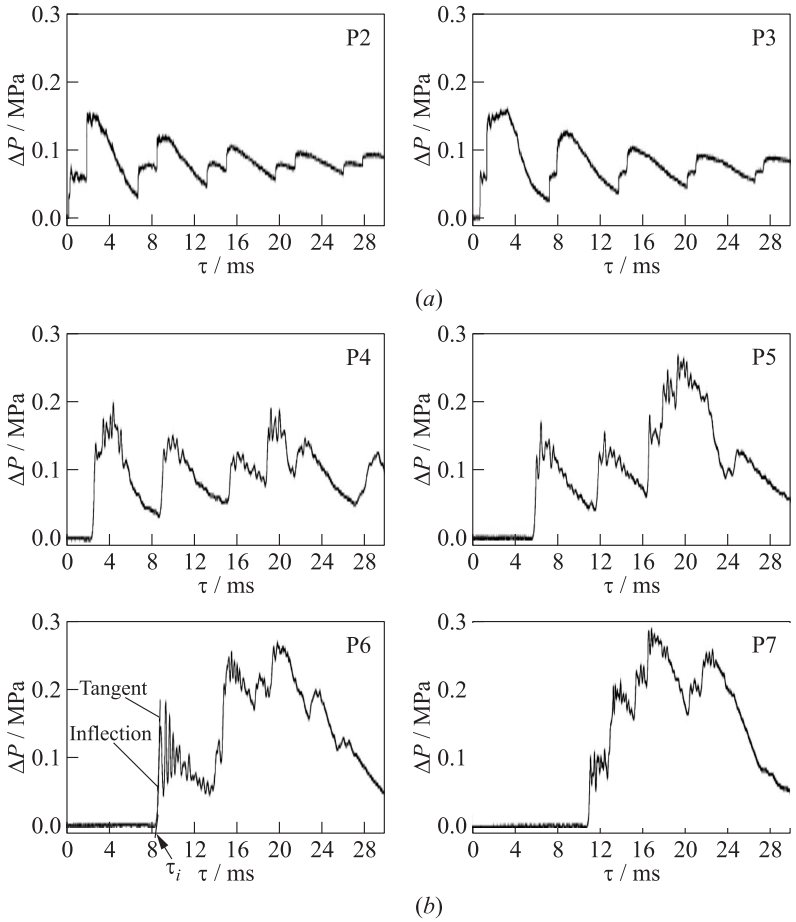

Figure 3 Representative pressure signals recorded with gauges P2–P7 for a volumetric gas content $\alpha_{10} = 0.04$ of "weak" SW ($\Delta P = 0.05$ MPa): (a) in gas; and (b) in bubbly liquid

an inflection point of the pressure record at its frontal part as shown in Fig. 3 for gauge P6.

As seen in Figs. 3 and 4, an oscillatory SW with a sloping front and regular pressure oscillations spreads through the bubbly liquid. Such

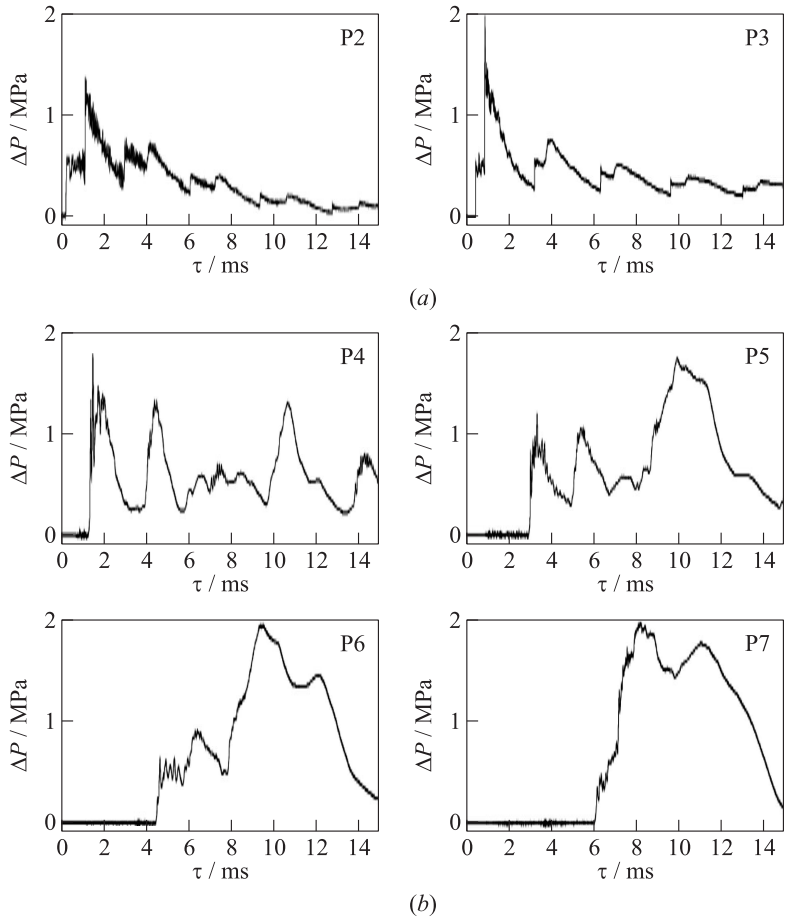

Figure 4 Representative pressure signals recorded with gauges P2–P7 for a volumetric gas content $\alpha_{10} = 0.04$ of "strong" SW ($\Delta P = 0.5$ MPa): (a) in gas; and (b) in bubbly liquid

waves have often been observed previously (see, e. g., [11, 16, 17]) and are associated with nonlinear and disperse properties of bubbly liquids. The time interval in Figs. 3 and 4 is quite long (18 and 8 ms in Figs. 3 and 4, respectively); therefore, the oscilloscopic traces exhibit not only

the primary SWs but SWs reflected from the closed tube ends and from the gas – bubbly liquid contact surface as well. Moreover, the oscilloscopic traces show also rarefaction waves.

Two-Phase Flow Models

Below, there will be considered bubbly liquid that consists of two phases, namely, dispersed gas phase (subscript 1) whose volume fraction is α_1 and carrier liquid phase (subscript 2) with volume fraction α_2. The following simplifying assumptions are adopted:

(1) gas compressed in an SW spreading through a bubbly liquid is not dissolved in the liquid while the liquid is not evaporated inside the bubbles;

(2) shock wave is of a moderate intensity, so that the liquid phase density depends solely on the liquid temperature T_2;

(3) flow of the bubbly liquid behind SW is laminar; and

(4) the effects of gravity, lifting, and friction forces at bounding surfaces on the relative phase motion in a bubbly liquid are ignored.

The mathematical models of SW interaction with a bubbly liquid are based on partial differential equations of mass, momentum, and energy conservation governing two-phase flows derived within the framework of mutually penetrating continua [11, 22]. The distinctive feature of the models is that in addition to the interphase exchange by momentum and energy, they take into account the effects of viscous tangential stresses and thermal fluxes in phases, which make the evolution problem well-posed [5–7].

Two models were applied. In Model 1, the pressures of phases were assumed identical ($p_2 = p_1$) and bubble diameter d_1 was assumed constant. In Model 2, the pressures of phases were assumed to be different due to the surface tension and relative motion between bubble and liquid, and the bubble diameter was assumed to vary according to the Rayleigh equation governing the volume oscillation of gas bubble in the liquid with the inertia of the added mass, difference of phase pressures, and viscous dissipation taken into account.

Numerical Method

The multiphase balance equations were solved numerically using AVL FIRE®. There, the discretization of the governing differential equations is obtained using a cell-centered finite volume approach. The governing equations are integrated, term by term, over the polyhedral control volumes. The method rests on the integral form of the general conservation law. All dependent variables such as volume fraction, density, velocity, pressure, and enthalpy are evaluated at the cell center. The cell-face-based connectivity and interpolation practices for gradients and cell-face values are introduced to accommodate an arbitrary number of cell faces. A second-order midpoint rule is used for integral approximation and a second-order linear approximation for any value at the cell face. The cell gradients can be calculated by using either the Gauss theorem or a linear least-square approach. The convection is solved by a variety of differencing schemes, namely, upwind, central differencing, and MINMOD. The time derivative is discretized by the implicit first-order accurate Euler (two levels) scheme.

After time integration, determination of the convection and diffusion terms, reorganization of the source terms, underrelaxation, and application of the boundary conditions, the outcome is a set of algebraic equations: one for each control volume and for each transport equation. Thus, for flow simulations with two phases applied in a computational domain with M control volumes, a system of $2 \times M \times N$ algebraic equations needs to be solved for N dependent variables. For the solution of the algebraic equation systems, the computational fluid dynamics (CFD) solver uses the iterative, preconditioned conjugate gradient method. The set of equations is solved in a sequence, meaning that each equation for a given variable is decoupled by treating the other variable as known.

Coupling between pressure and velocity is performed by the segregated SIMPLE-like (semiimplicit method for pressure linked equations) algorithm. The discrete continuity equations of the phases are combined to an overall continuity equation, and then are converted into an equation for the pressure correction. The pressure corrections are then used to update the pressure and velocity fields of the phases, so that the velocity components obtained from solution of the momentum equations satisfy the continuity equations.

Validation of the applied multiphase code in terms of bubbly flows with focus on boiling heat transfer can be found, e. g., in [23, 24]. The numerical method for solving Model 2 with additional equations is based on [25]. The numerical scheme used is monotone, which is necessary for problems with intrinsic physically nonmonotonous solutions. To perform numerical calculations accurately, the effect of mesh spacing and time step have been examined and appropriate values have been chosen.

Results and Discussion

Results of SW velocity measurements in bubbly water at measuring segment P5–P6 for "weak" and "strong" SWs at different volumetric gas content α_{10} values are shown in Fig. 5. For comparison, SW velocity vs. α_{10} calculated based on Models 1 and 2 with the aid of the aforedescribed techniques are also displayed by curves in Fig. 5.

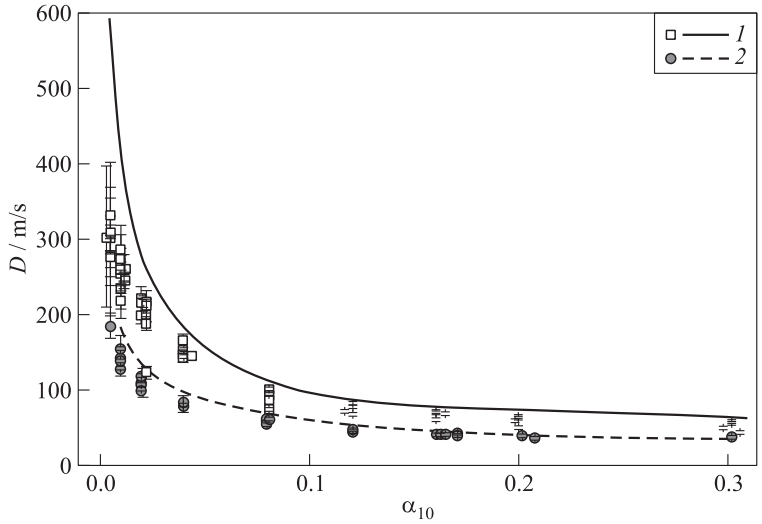

Figure 5 Shock wave velocities measured (signs) and calculated (curves) at measuring segment P5–P6 of HST setup vs. volumetric gas content in water: *1* — "strong" SWs; and *2* — "weak" SWs

Calculations were performed in 2D approximation for geometry simulating parameters of the HST of rectangular cross section. The procedure of theoretical assessment of the average SW velocity at the measuring segments was identical to that used in experiments. The differences in the calculated results in terms of the SW velocity were insignificant for the both models (they cannot be distinguished in the plot of Fig. 5). As seen in Fig. 5, the results of calculations agree quite well with measurements for "weak" SWs, whereas their consistency with experiment for "strong" SWs is satisfactory only at $\alpha_{10} > 0.04$–0.05. Furthermore, SW velocities in experiment decrease with distance faster than they do in calculations, although it should be emphasized that SW decay within the HST length is insignificant. This presumably can be accounted for by the fact that bubble breakup, which is more profound in "strong" SWs, is not included in the theoretical model.

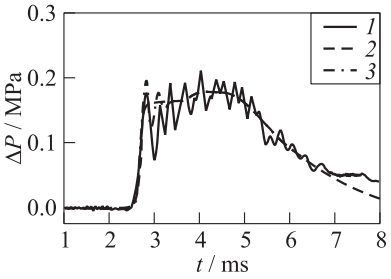

Figure 6 Comparison of pressure histories at the position of pressure gauge P4 predicted by two models with the experimental pressure record for the same initial conditions: $\alpha_{10} = 0.02$, "weak" SW; *1* — experiment; *2* — Model 1; and *3* — Model 2

Contrary to the SW velocity, the pressure profiles predicted by Model 1, on the one hand, and Model 2, on the other hand, differ from each other. As an example, Fig. 6 compares pressure histories at the position of pressure gauge P4 predicted by the two models with the experimental pressure record for the same initial conditions ($\alpha_{10} = 0.02$) for the weak SW. Model 1 predicts nonoscillating pressure history whereas Model 2 exhibits the oscillatory pressure behavior very similar to that observed experimentally. The predicted oscillation frequency correlates within 10% with the measured value with ≈ 2.7 kHz at $\alpha_{10} = 0.01$ and ≈ 3.7 kHz at $\alpha_{10} = 0.02$. For both calculations, the first few fluctuations are well consistent with experiment.

Further oscillations at the experimental pressure records can be caused by transverse motion of fluid due to pressure waves traversing

the channel in transverse direction. These pressure ways are not present in calculations.

Figures 7 and 8 show the example of predicted time histories of pressure (see Fig. 7) and normalized bubble radius (see Fig. 8) at po-

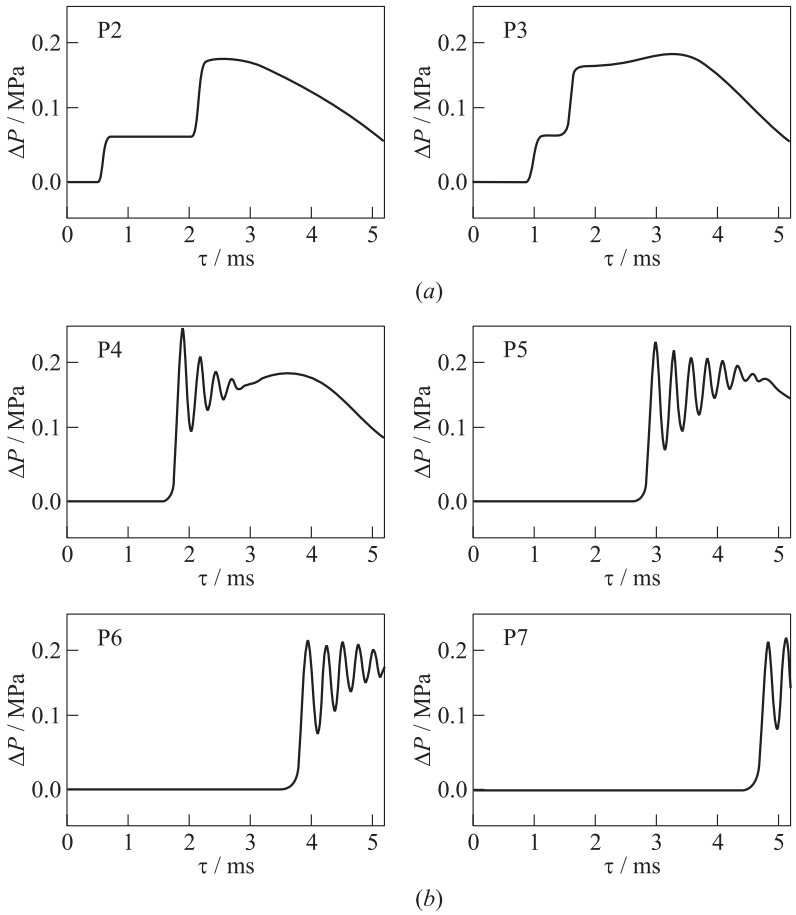

Figure 7 Calculated pressure at cross sections P2–P7 (volumetric gas content ~ 0.005, "weak" SW, $r_{10} = 1.25$ mm): (*a*) in gas; and (*b*) in bubbly liquid

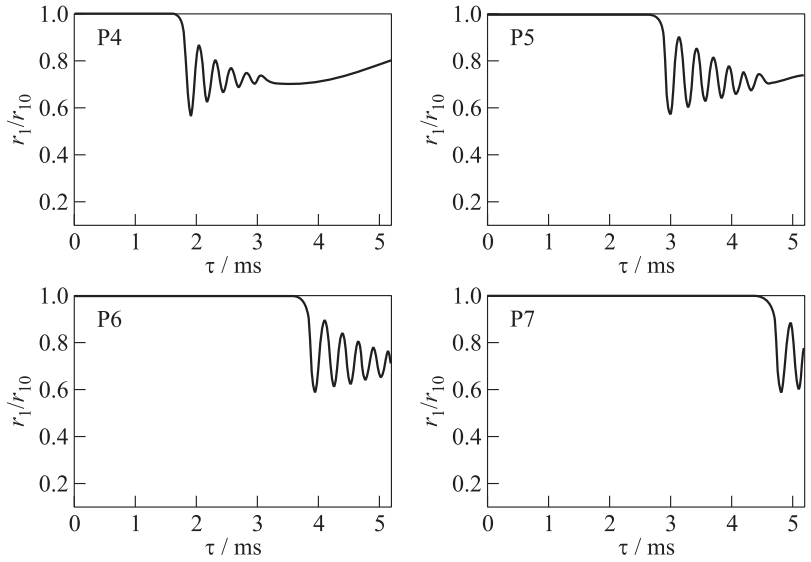

Figure 8 Calculated normalized bubble radius at cross sections P4–P7 (volumetric gas content ~ 0.005, "weak" SW, $r_{10} = 1.25$ mm)

sitions of gauges P2–P7 obtained by Model 2 for $\alpha_{10} \sim 0.005$ ("weak" SW). Decaying pressure oscillations are seen to be in phase with the decaying oscillations of normalized bubble radius.

Figure 9 shows the results of processing of the experimental and calculated data on the average velocity of the contact surface and the air bubble velocity in water with different gas content behind SWs of various intensity. Data on liquid motion (obtained based on the motion of polyethylene thread) are shown in Fig. 10. The average contact surface velocity is derived from videoframes based on information about the distance traveled by the interface during the time interval needed for SW to arrive at gauge P4. The air bubble velocity was assessed as its value at the moment when the SW arrives at gauge P4. The average velocity of the polyethylene thread is determined from a videorecord as its integral-average value within the time interval spanning from the instant when the tread starts moving to the instant when it stops.

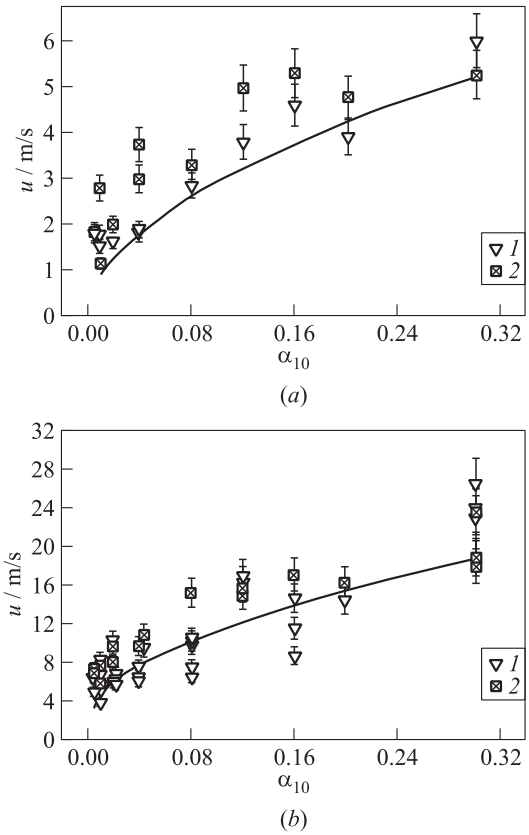

Figure 9 Measured (symbols) and calculated (curves) velocities of the contact surface (*1*) and air bubbles (*2*) behind "weak" ($\Delta P = 0.05$ MPa) (*a*) and "strong" ($\Delta P = 0.5$ MPa) (*b*) SWs vs. the initial volumetric gas content in water

The curves in the figure display the liquid velocities behind SW in the vicinity of its front calculated by Model 1.

As seen in Figs. 9 and 10 the measured velocities of the contact surface, air bubbles, and thread are qualitatively consistent quite well with each other. The large scatter of experimental data is presumably due

to several reasons including irregular distribution of bubbles over size and water volume, pressure oscillations caused by transverse and longitudinal waves both in LPS and TS, etc. The calculated liquid velocity agrees qualitatively with the experimental data and even quantitatively taking into account their scatter. Its experimental values in "strong" SWs at the highest gas content that deviate from the general trend call for further studies to be explained. The calculated fluid velocity behind SW rises as the gas content in water increases approximately proportionally to $\sqrt[n]{\alpha_{10}}$ with $n \sim 4$.

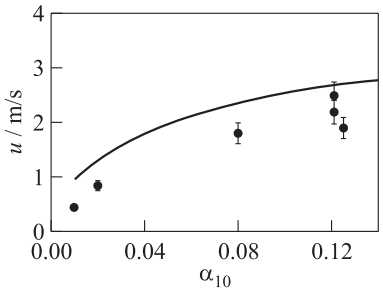

Figure 10 Measured average velocity of polyethylene thread (symbols) and calculated average velocity of liquid phase (curves) vs. the initial volumetric gas content in water for "weak" SWs with $\Delta P = 0.05$ MPa

Inasmuch as the liquid mass per unit volume of a bubbly liquid decreases monotonically as its gas content increases while the liquid velocity increases with gas content in the liquid, one should expect that the momentum imparted in the bubbly liquid by an incident SW as a function of gas content α_{10} should pass through a maximum or exhibit an asymptotic dependence.

The specific impulse acquired by a bubbly liquid behind an SW can be assessed by formula:

$$I = (1 - \alpha_{10})\rho_2 u_2$$

where ρ_2 is the water density assumed equal to 1000 kg/m^3 and u_2 is the liquid velocity behind SW that can be represented by the experimentally measured contact surface velocity or air bubble velocity behind SW.

The results of specific impulse calculations based on the experimental data discussed above are shown in Fig. 11 by symbols. The curves in Fig. 11 correspond to the specific impulse values calculated using the above described Model 1 (Model 2 provides very similar curves).

As follows from Fig. 11, the calculated specific impulse is well consistent with its values derived from experimental data within the entire

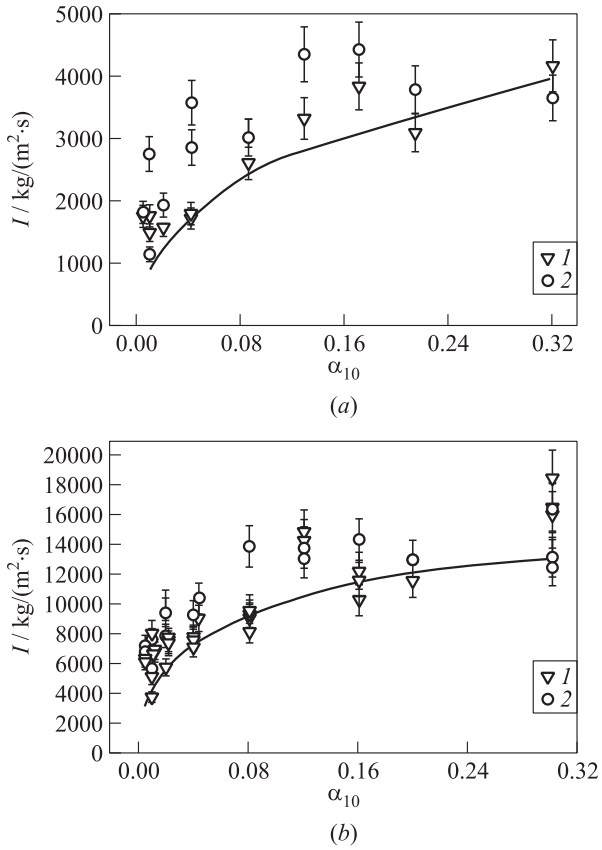

Figure 11 Measured (symbols) and calculated (curves) dependences of the specific impulse imparted in bubbly liquid by "weak" (*a*) and "strong" (*b*) SWs on the initial volumetric gas content: *1* — specific impulse assessed by the measured contact surface velocity; and *2* — specific impulse assessed by the measured air bubble velocity

range of the initial gas content tested. It is noteworthy that the specific impulse values imparted in a bubbly liquid by both "weak" and "strong" SWs tend to level off at an initial volumetric gas content of about 0.20–0.25, i. e., a further gas content increase changes the specific impulse value insignificantly.

Concluding Remarks

Systematic experimental and numerical investigations intended to ascertain the conditions, under which the efficiency of momentum transfer from an SW in air to bubbly water is the highest, are performed. Both experiments and calculations show that the momentum transfer efficiency attains its nearly maximum value at the volumetric gas content of about 0.20–0.25. As the volumetric gas content increases further (above 0.30), the amount of momentum transferred levels off. This latter finding would turn out to be of great importance in realization in practice of the detonation burning Zel'dovich cycle in various power units of water transport because it mitigates the requirements imposed on the accuracy of optimal gas content maintaining (at 0.20–0.25) in the water duct of, e. g., a hydrojet engine with no significant reduction of its operation efficiency. As the intensity of an incident SW increases, so does the impulse imparted in the two-phase liquid.

Acknowledgments

The work was supported by the Russian Ministry of Education and Science under the State Contract No. 14.609.21.0001 (Contract IDRFMEFI57914X0038).

References

1. Zel'dovich, Ya. B. 1940. K teorii rasprostraneniya detonatsii v gazoobraznykh sistemakh [On the theory of propagation of detonation in gaseous systems]. *Zh. Eksp. Teor. Fiz.* 10(5):542–568.
2. Frolov, S. M. 2006. Vvedenie [Introduction]. *Impul'snye detonatsionnye dvigateli* [Pulsed detonation engines]. Ed. S. M. Frolov. Moscow: TORUS PRESS. 19–22.
3. Roy, G. D., S. M. Frolov, A. A. Borisov, and D. W. Netzer. 2004. Pulse detonation propulsion: Challenges, current status, and future perspective. *Prog. Energ. Combust. Sci.* 30(6):545–672.
4. Frolov, S. M., F. S. Frolov, V. S. Aksenov, and K. A. Avdeev. 2013. Vodometnyy impul'snyy detonatsionnyy dvigatel' (varianty) i sposob sozdaniya gidroreaktivnoy tyagi [Water propulsion detonation engine (versions) and approach to generation of hydrojet

thrust]. Patent application PCT/RU2013/001148 on 23.12.2013 Available at: http://www.idgcenter.ru/patentPCT-RU2013-001148.htm (accessed June 20, 2016).

5. Avdeev, K. A., V. S. Aksenov, A. A. Borisov, R. R. Tukhvatullina, S. M. Frolov, and F. S. Frolov. 2015. Chislennoe modelirovanie vozdeystviya udarnoy volny na puzyr'kovuyu sredu [Numerical modeling of the impact of shock wave on bubbly environment]. *Goren. Vzryv (Mosk.) — Combustion and Explosion* 8(2):45–56.
6. Avdeev, K. A., V. S. Aksenov, A. A. Borisov, R. R. Tukhvatullina, S. M. Frolov, and F. S. Frolov. 2015. Chislennoe modelirovanie peredachi impul'sa ot udarnoy volny k puzyr'kovoy srede [Numerical simulation of the momentum transfer from the shock waves to the bubble media]. *Goren. Vzryv (Mosk.) — Combustion and Explosion* 8(2):57–67.
7. Avdeev, K. A., V. S. Aksenov, A. A. Borisov, R. R. Tukhvatullina, S. M. Frolov, and F. S. Frolov. 2015. Numerical simulation of momentum transfer from a shock wave to a bubbly medium. *Russ. J. Phys. Chem. B* 9(3):363–374.
8. Mory, J., K. Hijikata, and A. Komine. 1975. Propagation of pressure waves in two-phase flow. *Int. J. Multiphase Flow* 2:139–152.
9. Nakoryakov, V. E., B. G. Pokusaev, I. R. Shraiber, V. V. Kuznetsov, and N. V. Malykh. 1975. Eksperimental'noe issledovanie udarnykh voln v zhidkosti s puzyr'kami gaza [Experimental study of shock waves in the liquid with gas bubbles]. *Volnovye protsessy v dvukhfaznykh sistemakh* [Wave processes in two-phase systems]. Ed. S. S. Kutateladze. Novosibirsk: Institute of Thermophysics SB USSR AS. 54–97.
10. Kalra, S. P., and Y. Zvirin. 1981. Shock wave-induced bubble motion. *Int. J. Multiphase Flow* 7(1):115–127.
11. Kutateladze, S. S., and V. E. Nakoryakov. 1984. *Teplomassoobmen i volny v gazozhidkostnykh sistemakh* [Heat and mass transfer and waves in gas–liquid systems]. Novosibirsk: Institute of Thermophysics SB USSR AS. 301 p.
12. Sytchev, A. I. 2010. Sil'nye udarnye volny v puzyr'kovykh sredakh [Strong shock waves in bubbly media]. *Russ. J. Techn. Phys.* 80(6):31.
13. Noordzij, L. V. 1973. Shock waves in bubble–liquid mixtures. *Neustanovivshiesya techeniya vody s bol'shimi skorostyami* [Unsteady water flows with high velocities]. Moscow: Nauka. 369–383.
14. Gel'fand, B. E., S. A. Gubin, B. S. Kogarko, and S. M. Kogarko. 1973. Issledovanie voln szhatiya v smesi zhidkosti s puzyr'kami gaza [Investigations of compression waves in a mixture of liquid with gas bubbles]. *Dokl. Akad. Nauk* 213(5):1043–1046.

15. Kotchetkov, I. I., and A. V. Pinaev. 2012. Shock and detonation waves generated by a wire explosion in liquid and bubbled media. *Combust. Explo. Shock Waves* 48(2):236–244.
16. Burdukov, A. P., V. V. Kuznetsov, S. S. Kutateladze, V. E. Nakoryakov, B. G. Pokusaev, and I. R. Shreiber. 1971. Udarnaya volna v gazozhidkostnoy srede [Shock wave in a gas–liquid medium]. *J. Appl. Mech. Tech. Phys.* 3:65–69.
17. Noordzij, L. 1971. Shock waves in bubble-liquid mixtures. *Phys. Commun. Twente Univ. Tech.* 3(1):52.
18. Kedrinskii, V. K., and R. I. Soloukhin. 1961. Szhatie sfericheskoy gazovoy polosti v vode udarnoy volnoy [Compression of spherical gas cavity by a shock wave]. *J. Appl. Mech. Tech. Phys.* 1:27–29.
19. Voinov, O. V., and A. G. Petrov. 1971. Dvizhenie sfery peremennogo ob"ema v ideal'noy zhidkosti okolo tverdoy poverkhnosti [Movement of a sphere of variable volume in an ideal fluid around the solid surface]. Izv. Akad. Nauk Fluid Dynamics 5:94–103.
20. Kedrinskii, V. K. 1980. Shock waves in a liquid containing gas bubbles. *Combust. Explo. Shock Waves* 16(5):495–504.
21. Ranjan, D., J. Oakley, and R. Bonazza. 2011. Shock–bubble interactions. *Annu. Rev. Fluid Mech.* 43:117–140.
22. Nigmatulin, R. I. 1990. *Dynamics of multiphase media*. New York, NY: Hemisphere. Vol. 1. 464 p.
23. Srinivasan, V., K. M. Moon, D. Greif, D. M. Wang, and M. W. Kim. 2010. Numerical simulation of immersion quench cooling process using an Eulerian multi-fluid approach. *Appl. Thermal Eng.* 30(5):499–509.
24. Kopun, R., L. Skerget, M. Hribersek, Zhang D. Dongsheng, B. Stauder, and D. Greif. 2014. Numerical simulation of immersion quenching process for cast aluminium part at different pool temperatures. *Appl. Thermal Eng.* 65:74–84.
25. Kameda, M., and Y. Matsumoto. 1996. Shock waves in a liquid containing small gas bubbles. *Phys. Fluids* 8(2): 322–335.